



UNICA

UNIVERSITÀ
DEGLI STUDI
DI CAGLIARI



Università di Cagliari

UNICA IRIS Institutional Research Information System

This is the Author's *accepted* manuscript version of the following contribution:

Biolatti M., et al., Strigolactones as broad-spectrum antivirals against β -coronaviruses through targeting the main protease Mpro, ACS Infectious Diseases, 9, 2023, pagg. 1310-1318

The publisher's version is available at:

<https://doi.org/10.1021/acsinfecdis.3c00219>

When citing, please refer to the published version.

This full text was downloaded from UNICA IRIS <https://iris.unica.it/>

Strigolactones as broad-spectrum antivirals against β -coronaviruses through targeting the main protease M^{pro}

Matteo Biolatti^a, Marco Blangetti^b, Melissa Baggieri^c, Antonella Marchi^c, Silvia Gioacchini^c, Greta Bajetto^{a,d}, Davide Arnodo^b, Paola Bucci^c, Raoul Fioravanti^c, Maedeh Kojouri^c, Matteo Bersani^c,

Giulia D'Arrigo^c, Lydia Siragusa^{f,g}, Simone Ghinato^b, Marco De Andrea^{a,d}, Francesca Gugliesi^a, Camilla Albano^a, Selina Pasquero^a, Ivan Visentin^h, Emilio D'Ugo^c, Francesca Espositoⁱ, Paolo Maluneⁱ, Enzo Tramontanoⁱ, Cristina Prandi^b, Francesca Spyrakis^{c*}, Fabio Magurano^{c*}, Valentina Dell'Oste^{a*}.

^aDepartment of Public Health and Pediatric Sciences, University of Turin, 10126 Turin, Italy.

^bDepartment of Chemistry, University of Turin, 10125 Turin, Italy.

^cDepartment of Infectious Diseases, Istituto Superiore di Sanità, 00161 Rome, Italy.

^dCenter for Translational Research on Autoimmune and Allergic Disease-CAAD, 28100 Novara, Italy.

^eDepartment of Drug Science and Technology, University of Turin, 10125 Turin, Italy.

^fMolecular Discovery Ltd., Kinetic Business Centre, Elstree, Borehamwood, WD6 4PJ Hertfordshire, United Kingdom.

^gMolecular Horizon s.r.l., 06084 Bettona (PG), Italy.

^hDepartment of Agricultural, Forestry, and Food Sciences, University of Turin, 10095 Grugliasco, Turin, Italy.

ⁱDepartment of Life and Environmental Sciences, University of Cagliari, 09042 Monserrato, Cagliari, Italy.

*Corresponding authors. fabio.magurano@iss.it; francesca.spyrakis@unito.it; valentina.delloste@unito.it

ABSTRACT

The current SARS-CoV-2 pandemic and the likelihood that new coronavirus strains will emerge in the immediate future point out the urgent need to identify new pan-coronavirus inhibitors. Strigolactones (SLs) are a class of plant hormones with multifaceted activities whose role in plant-related fields has been extensively explored. Recently, we proved that SLs also exert an antiviral activity toward herpesviruses, such as human cytomegalovirus (HCMV). Here we show that the

synthetic SLs TH-EGO and EDOT-EGO impair β -coronavirus replication, including SARS-CoV-2 and the common cold human coronavirus HCoV-OC43. Interestingly, *in-silico* simulations suggest the binding of SLs in the SARS-CoV-2 main protease (M^{pro}) active site, and this was further confirmed by an *in-vitro* activity assay. Overall, our results highlight the potential efficacy of SLs as broad-spectrum antivirals against β -coronaviruses, which may provide the rationale for repurposing this class of hormones for the treatment of COVID-19 patients.

KEYWORDS

Antiviral screening, Strigolactones, HCoV-OC43, SARS-CoV-2, M^{pro}

Emerging coronaviruses (CoVs) have recently raised global concerns, due to their high spillover potential and transmissibility rate, worsened by the limited availability of effective treatments¹. Although a series of drugs approved for clinical use effectively inhibits severe acute respiratory syndrome coronavirus-2 (SARS-CoV-2) infection *in-vitro*², there is an urgent requirement for broad-spectrum antivirals.

Recently, the use of traditional medicines as an adjuvant in the treatment of COVID-19 has been demonstrated³. Strigolactones (SLs) are an emerging class of plant hormones with many functions^{4,5}. They are made up of a tricyclic ABC core linked through an enol ether bridge to a fourth butenolide ring, commonly known as the D-ring, responsible for the bioactivity of SLs⁵. While their role in plant-related fields has been exhaustively investigated, the effects of SLs on human cells and their potential use in medicine are still poorly defined. So far, the most significant data on SLs suggest they have the ability to induce G2/M arrest and apoptosis in various types of human cancer cells^{6,7}. Additionally, recent research shows that SLs may have promising anti-inflammatory properties by inhibiting the release of inflammatory molecules and the migration of

neutrophils and macrophages in zebrafish larvae, as well as by increasing detoxifying enzymes^{8–10}. Recently, we proved that SLs also exert an antiviral activity toward herpesviruses¹¹.

Based on this background, this work aimed to ascertain whether SLs might constitute a new class of broad-spectrum compounds against β -CoV_S.

We employed two indole-based SL analogs, named TH-EGO and EDOT-EGO (Figure 1A), derived from the potent antioxidant and neuroprotectant tryptophan metabolite indole-3-propionic acid¹². The hydrolytic stability of TH-EGO and EDOT-EGO in the prototypical DMEM/FBS 10% culture medium was evaluated (Figure 1B). Both compounds follow an exponential model decay and show comparable hydrolytic stabilities with estimated half-life times of 11.96 h for TH-EGO and 10.54 h for EDOT-EGO.

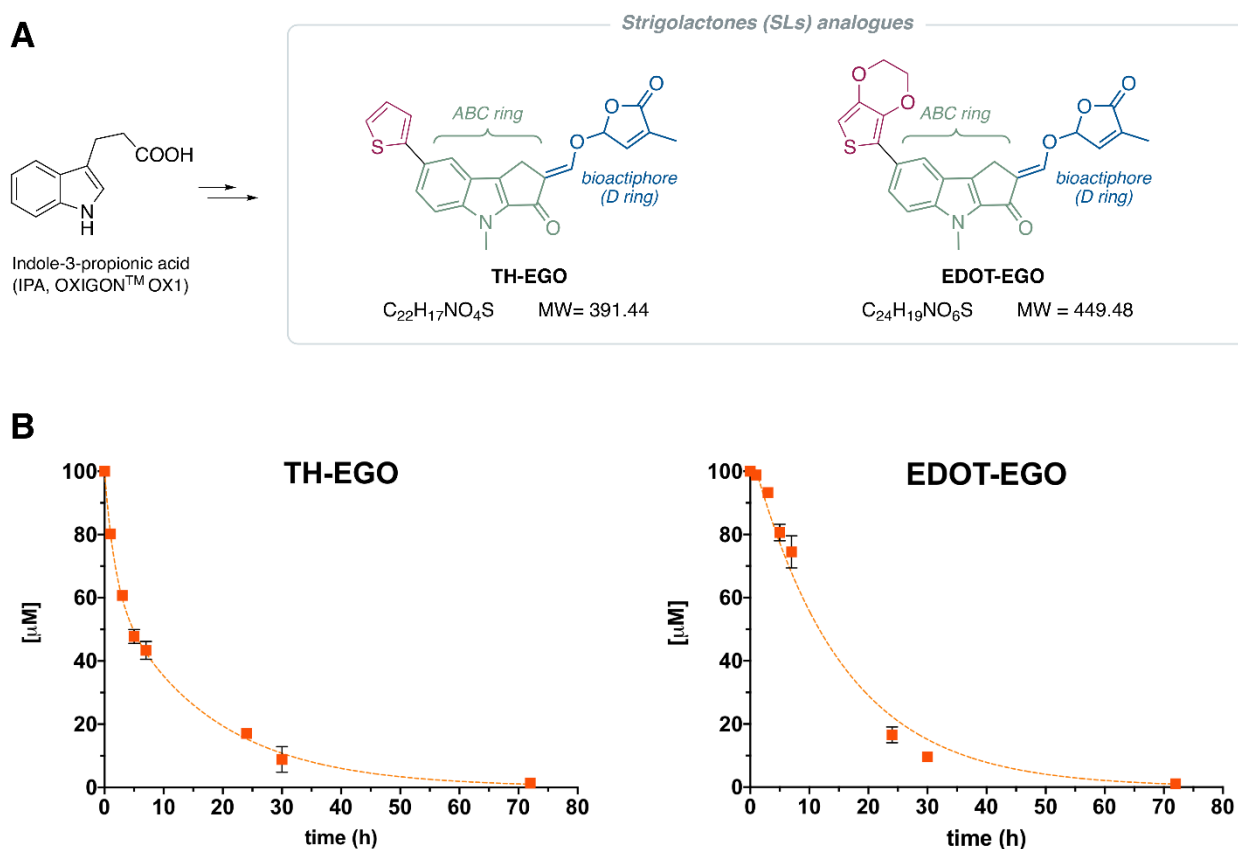


Figure 1. Indole-derived SL analogs. (A) Chemical structures of TH-EGO and EDOT-EGO. (B) Stability analyses of TH-EGO and EDOT-EGO in culture medium. $[SL]_0 = 100 \mu M$ in DMEM/FBS + 0.5% DMSO. RP-HPLC analyses were run on an endcapped C18 (150 x 4.6 mm ID, 5 μM) column, using acetonitrile/H₂O (60/40 v/v) as a solvent mixture (1 mL/min flow rate) and analyzed

at 295 nm (TH-EGO) and 326 nm (EDOT-EGO). Bars show means \pm SEM of three independent experiments.

Initial screening to assess the antiviral activity of TH-EGO and EDOT-EGO was performed using HCoV-OC43 due to its low biosafety concerns. First, a standard MTT viability assay was employed to rule out any cytotoxic effect of the compounds on MRC-5 cells. Both compounds' cytotoxicity for MRC-5 was low or undetectable at concentrations up to 25 μ M, since ~90 % of cells were viable after 48 h of treatment (Figure 2A).

Then, TH-EGO and EDOT-EGO were analyzed for their antiviral activity against HCoV-OC43 at a concentration of 25 μ M, which was the minimum effective dose that did not show remarkable cytotoxicity. The antiviral activity was first measured on infected MRC-5 cells by RT-PCR. In this test, the inhibitory effect of a compound on viral replication is calculated by relative quantitation of the viral RNA genome released in supernatants in the presence of the compound *vs.* the vehicle control (DMSO). As shown in Figure 2B, both tested SLs demonstrated significant inhibitory activity against HCoV-OC43. According to the results obtained measuring viral RNA released in the supernatants, SLs also reduced the intracellular viral genome (Figure 2C), suggesting they act during the replication of the virion and not in the maturation step. Additionally, we investigated the effects of TH-EGO and EDOT-EGO on the HCoV-OC43 nucleocapsid protein (N) expression by Western blotting. Interestingly, both compounds significantly reduced HCoV-OC43 N protein expression, thus confirming their inhibitory activity during the replication phase (Figure 2D).

Finally, a more detailed analysis with serial dilutions of the two compounds revealed that both TH-EGO and EDOT-EGO specifically inhibited HCoV-OC43 replication in a dose-dependent manner when the compounds were added to the cells 2 h before, during, and after infection (Figure 2E, panel i). To deeply understand which phase of the viral replication cycle is targeted by SL analogs, the compounds were added to the cells during the adsorption stage (Figure 2E, panel ii) or after the removal of inoculum (post-adsorption stage) (Figure 2E, panel iii). The virus yield reduction assay

revealed that TH-EGO and EDOT-EGO retained a significant activity against HCoV-OC43 when added after the infection, but not during the adsorption stage, suggesting that SL analogs interfere with a late molecular event during HCoV-OC43 replication cycle.

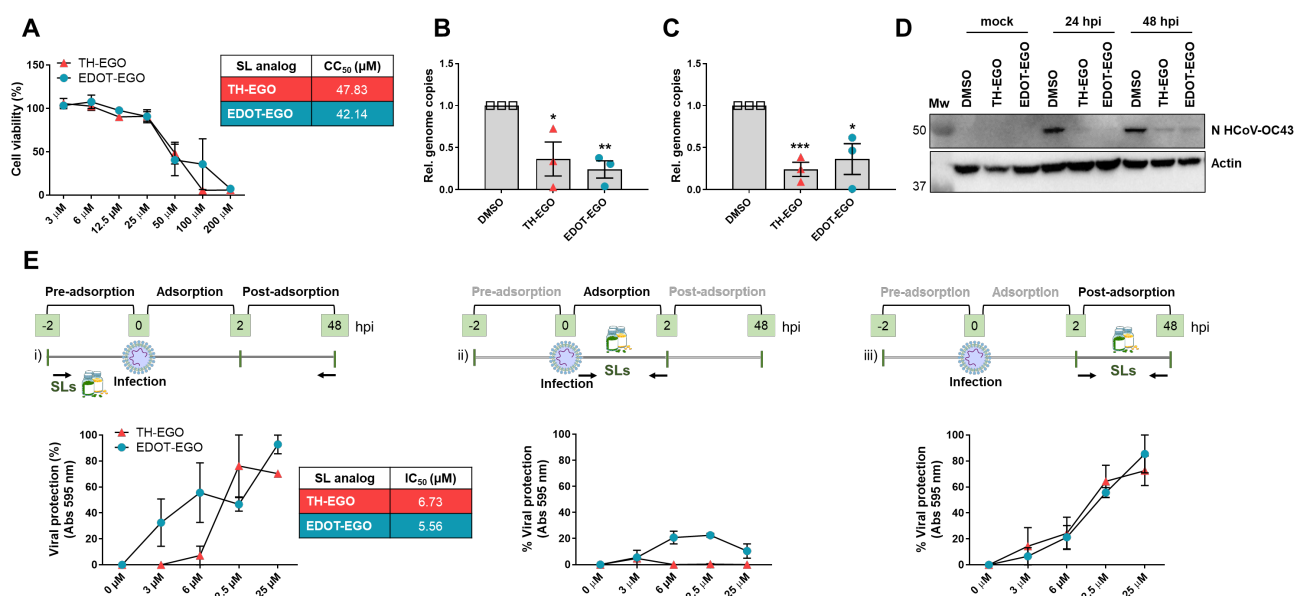


Figure 2. SL analogs as antivirals against HCoV-OC43. (A) Cell viability was measured using the MTT assay. Confluent MRC-5 cultures were incubated with different concentrations of the indicated SLs for 48 h. Bars show means \pm SEM of three independent experiments. CC₅₀ values are reported in the table. (B) MRC-5 cells were pre-treated with 25 μ M of the indicated SLs or vehicle (DMSO) for 2 h. Later, MRC-5 were infected with HCoV-OC43 (MOI 0.1), and following virus adsorption (2 h at 33°C), the viral inoculum was removed, and cultures were exposed to the compounds. At 48 hpi the number of HCoV-OC43 genomes released in the supernatants of infected cells was measured by RT-PCR. The mean value of DMSO-treated cells was arbitrarily set to 1. Bars show means \pm SEM of three independent experiments ($P < 0.05^*$; $P < 0.01^{**}$; unpaired t-test, for comparison of SL vs. DMSO-treated cells). (C) The cells from (B) were also used to determine the relative intracellular number of viral RNA genomes in infected cells. The mean value of DMSO-treated cells was arbitrarily set to 1. Bars show means \pm SEM of three independent experiments ($P < 0.05^*$; $P < 0.001^{***}$; unpaired t-test, for comparison of SL vs. DMSO-treated

cells). (D) Western blot analysis of protein lysates from uninfected (mock) or infected cells using antibodies against HCoV-OC43 N protein or Actin. One representative blot (left panel) and densitometric analysis (right panel) are shown. Values are expressed as the percentage of inhibition of HCoV-OC43 N protein expression normalized to Actin (DMSO-treated cells were arbitrarily set to 100). (E) Time-of-addition assays. MRC-5 cells were: i) pre-treated with serial dilutions of SLs for 2 h. Later, MRC-5 were infected with HCoV-OC43 (MOI 0.1) in the presence of the compounds, and following virus adsorption (2 h at 33°C), the viral inoculum was removed, cultures were exposed to increasing dilutions of SLs or vehicle (DMSO) and incubated for 48 h. IC₅₀ values are reported in the table. ii) The compounds and the virus were added simultaneously on cells (2 h at 33°C) and then removed. iii) MRC-5 were infected with HCoV-OC43 as described above and after the removal of inoculum they were treated with increasing concentrations of the compound and incubated for 48 h. Supernatants were harvested, and infectivity titers were determined by colorimetric plaque assay. Bars show the means \pm SEM of three independent experiments.

To verify if SL derivatives maintain their antiviral activity also toward other β -CoVs, we examined the impact of SL treatment on SARS-CoV-2 replication. The cytotoxicity of TH-EGO and EDOT-EGO for VERO E6 was low or undetectable at concentrations up to 200 μ M (Figure 3A). First, TH-EGO and EDOT-EGO were analyzed for their antiviral activity against SARS-CoV-2 at a concentration of 25 μ M (*i.e.*, the same doses used for HCoV-OC43 experiments) by RT-PCR. As shown in Figure 3B, both tested SLs retained their antiviral activity also against SARS-CoV-2. Then, a more detailed analysis with serial dilutions of the two compounds revealed that the two compounds impair SARS-CoV-2 replication on VERO E6 cells in a dose-dependent manner when the compounds were added to the cells 2 h before, during, and after infection (Figure 3C, panel i). It is worth noting that also in the SARS-CoV-2 model, SLs demonstrate sustained antiviral effects when added after the removal of inoculum during the post-adsorption stage (Figure 3C, panel iii). This observation is consistent with our findings for HCoV-OC43 (Figure 2E). Conversely, SLs do

not exhibit efficacy when inoculated during the adsorption stage (Figure 3C, panel ii), providing further evidence that a late step of β -CoV replication is targeted by SLs.

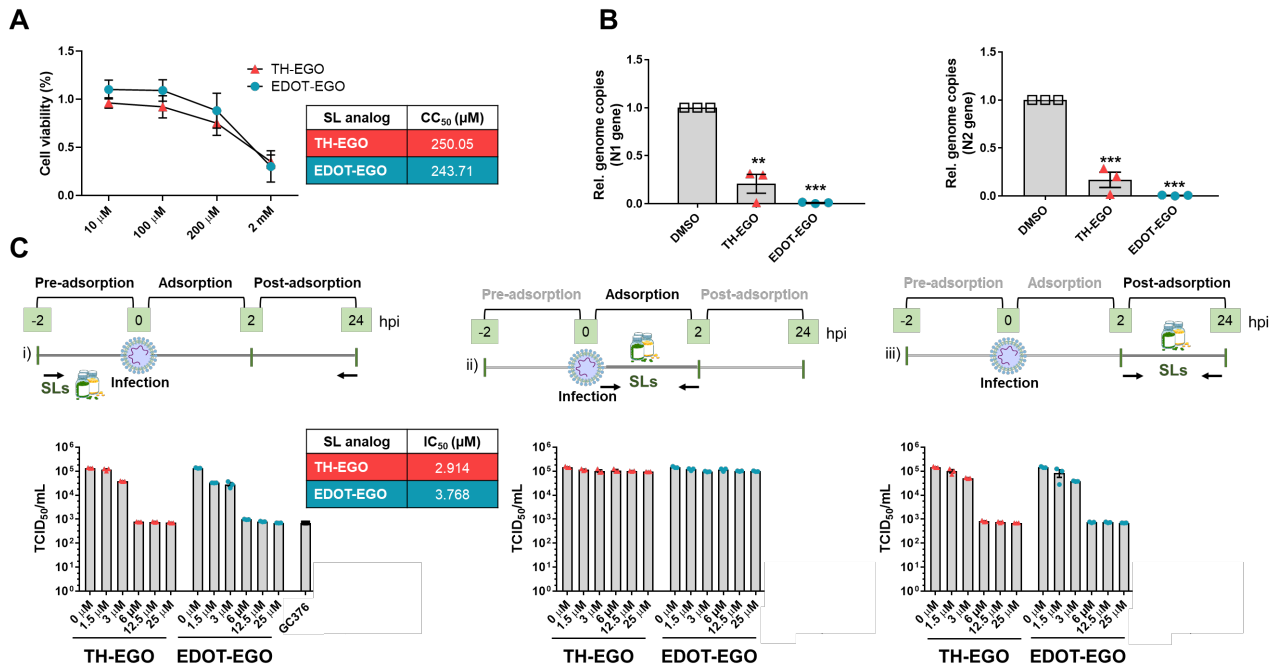


Figure 3. SL analogs as antivirals against SARS-CoV-2. (A) Cell viability was determined using the XTT assay. Confluent VERO E6 cultures were incubated with different concentrations of the indicated SLs for 24 h. Bars show the mean \pm SD of three independent experiments. CC₅₀ values are reported in the table. (B) VERO E6 cells were pre-treated with the indicated SLs (25 μ M) or vehicle (DMSO) for 2 h and then infected with SARS-CoV-2 (MOI 0.01). Following virus adsorption (2 h at 37°C), the viral inoculum was removed, and cultures were exposed to SLs or DMSO. At 24 hpi the number of SARS-CoV-2 genomes leased in the supernatants of infected cells was measured by RT-PCR (N1, left panel, and N2, right panel). The mean value of DMSO-treated cells was arbitrarily set to 1. Bars show means \pm SEM of three independent experiments ($P < 0.05^*$; $P < 0.01^{**}$; $P < 0.001^{***}$; unpaired t-test, for comparison of SL vs. DMSO-treated cells). (C) VERO E6 cells were i) treated with serial dilutions of SLs for 2 h. Later, cells were infected with SARS-CoV-2 in the presence of the compounds, and following virus adsorption (2 h at 37°C), the viral inoculum was removed, cultures were exposed to increasing dilutions of SLs or vehicle

(DMSO) and incubated for 24 h. IC₅₀ values are reported in the table. ii) The compounds and the virus were added simultaneously on cells (2 h at 37°C) and then removed. iii) VERO E6 were infected with SARS-CoV-2 and after the removal of inoculum they were treated with increasing concentrations of the compounds and incubated for 24 h. Supernatants were harvested, and the 50% end-point titers (TCID₅₀) were determined using the Spearman-Kärber method. Bars show the means ± SEM of three independent experiments. GC376 (5 µM)¹³ was used as a positive control of antiviral activity.

To investigate which SARS-CoV-2 protein could be targeted by the analyzed SLs, we screened both SLs towards all the structures of coronavirus proteins present in CROMATIC at the time of the analyses¹⁴, using the screening procedure that allows evaluating the possible interaction of a series of ligands with several protein pockets. Overall, a total amount of 67 proteins and 124 pockets, belonging to the viruses MERS-CoV, SARS-CoV-1, and SARS-CoV-2, were considered¹⁴. Pockets were ranked according to the Glob-Prod score and selected for having a score higher than 1.

Among the highest-scored pockets of SARS-CoV-2, we noticed the presence of the 3-chymotrypsin-like protease (3CL^{pro}) or main protease (M^{pro}) orthosteric site, characterized by a Cys-His catalytic dyad. In particular, M^{pro} was identified at the fourth position among SARS-CoV-2 proteins, after the nucleoprotein C terminal domain, Nsp12, and Nsp14 (see Table S1). Preliminary *in-silico* docking simulations showed the most promising poses of both SLs in M^{pro}, in terms of the number of interactions and stability of the poses.

These findings align with the observation that M^{pro} is currently one of the primary targets of several antivirals, including Nirmatrelvir (the active component of Paxlovid)¹⁵, Ensitrelvir¹⁶, and Simnotrelvir¹⁷, which have already received clinical approval in certain countries and regions worldwide. Moreover, M^{pro} is a promising target also considering the SL mechanism of action. Indeed, the natural target of SLs in plants, and specifically in rice, is an α/β -fold hydrolase named DWARF 14 (D14)¹⁸, which hydrolyzes SLs into the active form of hormone (CLIM), covalently

binds CLIM to trigger SL signaling and finally release an inactive hydrolysis product. The hydrolysis is performed by a Ser/His/Asp catalytic triad, which operates a nucleophilic attack on the ring D cyclic ester, as proposed by Scaffidi et al.¹⁹. Similarly, M^{pro} could hydrolyze SLs by a nucleophilic attack performed by the deprotonated catalytic cysteine²⁰.

We, thus, performed a more accurate docking simulation of EDOT-EGO and TH-EGO in M^{pro} binding site with Gold, obtaining similar and reasonable poses for both ligands (Figure 4A, C). In particular, for both compounds, a H-bond is formed between His163 and the lactone D-ring carbonyl group, while several hydrophobic contacts involve Met49, Met165, and Pro168 and the other SL rings. Interestingly, the interaction with His163 appears to be crucial for properly targeting M^{pro} active site²¹, and the lactone functionality of the D-ring is close to the catalytic Cys145, thus supporting the hypothesis of a subsequent possible covalent attack. The docking score, provided by the PLP scoring function for the reported EDOT-EGO and TH-EGO, was over 60, thus supporting the prediction reliability²². Similar results were obtained when docking the compounds in M^{pro} from HCoV-OC43 (Figure S1).

We then simulated a covalent docking for both SLs in M^{pro} with Glide, obtaining the adducts reported in Figures 4B, D, and S2. In particular, we simulated the catalytic mechanism proposed by Scaffidi et al.¹⁹, in which the cysteine attacked the lactone moiety (Figure S3), the ABC ring has been released and a receptor-ligand covalent intermediate, stabilized by an additional H-bonds, has formed (Figure 4B, D).

We thus hypothesized that both SLs could recognize M^{pro} binding site to form a non-covalent complex, subsequently transforming into a covalent intermediate.

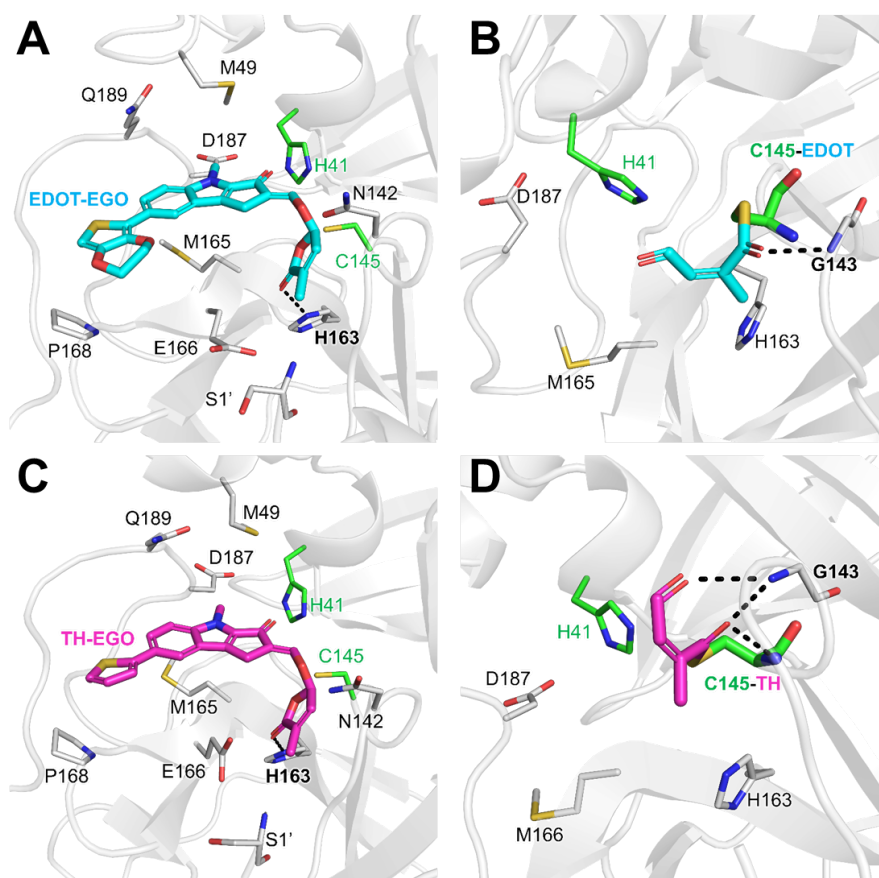


Figure 4. SARS-CoV-2 M^{pro} is targeted by SLs. (A, C) Docking poses of EDOT-EGO (A) and TH-EGO (C) in M^{pro}. (B, D) Second intermediate covalent adduct of EDOT-EGO (B) and TH-EGO (D) in M^{pro} obtained by covalent docking. The protein is shown as a cartoon, and the ligand and the key residues in the binding site are labeled and shown as capped sticks. H-bonds are displayed as black dashed lines.

To validate the computational results, we tested EDOT-EGO and TH-EGO on SARS-CoV-2 M^{pro} activity, using a biochemical assay. Serial dilutions of compounds were incubated with M^{pro} and a substrate peptide was added. The resulting fluorescence resonance energy transfer (FRET) signal was acquired after 15 minutes of cleaving reaction at room temperature. GC376 was used as a positive control²³.

Both compounds TH-EGO and EDOT-EGO were able to inhibit the activity of the SARS-CoV-2 M^{pro} and showed an IC₅₀ value in the nanomolar range (0.008 μ M and 0.048 μ M, respectively) (Figure 5). To assess the broad-spectrum effect of SL analogs, we tested EDOT-EGO and TH-EGO

on MERS-CoV M^{pro} activity. MERS-CoV is another β -coronavirus that shares 50.3% of M^{pro} sequence identity with SARS-CoV-2²¹. Both compounds were able to inhibit also the activity of the MERS M^{pro}, but with less potency (Figure S4). For clarity, it should be noted that the IC₅₀ of GC376 is 0.00013 μ M, while the concentration of M^{pro} enzyme used in the reaction is 15 nM, which represents the optimal enzyme concentration based on enzyme kinetics for the assay. However, it is worth noting that this concentration exceeds the inhibitor concentration by more than 10-fold. Hence, it is reasonable to speculate that only a fraction of the enzyme molecules are active during the evaluation of the compound inhibition capability. Consequently, it can be inferred that the concentration of GC376 required to inhibit 50% enzyme activity is less than 50% of the total protein concentration. To further confirm the predicted inhibitory mechanism of action of EDOT-EGO and TH-EGO on SARS-CoV-2 M^{pro} activity, we performed the biochemical assay as previously described, with different pre-incubation times of the enzyme in the reaction mix in the presence of compounds, before the addition of the substrate. Results in Figure 5, panel D, show an increase in the IC₅₀ value when increasing the pre-incubation time, similarly to what was observed for the control GC376, suggesting a covalent reversible inhibitory mode of action for both tested compounds²⁴.

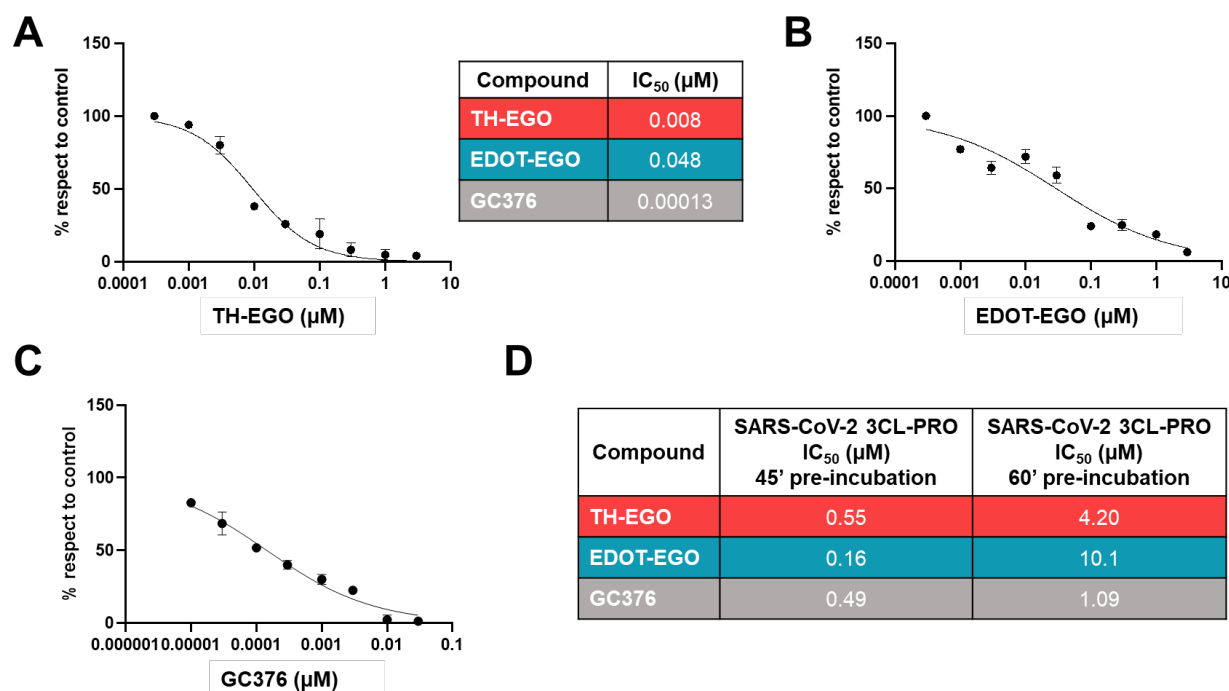


Figure 5. Inhibitory effect of SL analogs on SARS-CoV-2 M^{pro} activity. Inhibition curves of SARS-CoV-2 M^{pro} by TH-EGO (A), EDOT-EGO (B), and GC376 (C). (D) Influence of longer preincubation times of the SL analogs on SARS-CoV-2 M^{pro} activity. GC376 was used as a positive control. IC₅₀ values are reported in the table.

Overall, our findings show that the SL TH-EGO and EDOT-EGO inhibit the replication of both HCoV-OC43 and SARS-CoV-2. Importantly, *in-silico* simulations and activity experiments revealed that SARS-CoV-2 M^{pro} is targeted and inhibited by both molecules. Our studies allowed the discovery of potential antiviral compounds for further testing *in-vivo* to contain the current outbreak. Additionally, it may aid in the development of pan-anti-CoV inhibitors/treatments that can quickly and effectively respond to future pandemics.

METHODS

Compounds. The SL analogs TH-EGO and EDOT-EGO, synthesized as previously described²⁵, were dissolved in dimethyl sulfoxide (DMSO) (Sigma-Aldrich) at stock concentrations of 20 mM and used as racemic mixtures. The GC376 compound (DBA Italia) was dissolved in DMSO and used as a positive control in SARS-CoV-2 antiviral assays and M^{pro} *in-vitro* activity assay.

Hydrolytic stability of SL analogs. The hydrolytic stability of TH-EGO and EDOT-EGO was evaluated by incubation in Dulbecco's Modified Eagle Medium (DMEM; Sigma-Aldrich) supplemented with 10% (v/v) fetal bovine serum (FBS; Sigma-Aldrich). The stock solution of the compound (20 mM in DMSO) was diluted in preheated (37°C) DMEM/FBS (10%) to a final concentration of 100 μ M. The solution was incubated at $37 \pm 0.5^\circ\text{C}$ and at appropriate time intervals a 300 μ L aliquot of mixture was withdrawn and added to 300 μ L of acetonitrile (+0.1% HCOOH) to deproteinize the serum. The sample was sonicated, vortexed, filtered through 0.45 μ m PTFE filters (Alltech), and analyzed by RP-HPLC. All experiments were performed in triplicate. RP-HPLC analyses were performed with a Waters 1500 chromatograph system (Waters, Milford, MA, USA) equipped with a manual injector (Rheodyne, Cotati, CA, USA), a binary pump (model 1525), a diode-array detector (DAD, model 2998) integrated into the Waters system. The injection volume was 20 μ L. Analyses were performed on a SunFireTM endcapped C18 column (150 x 4.6 mm ID, 5 μ m) using an acetonitrile/water mobile phase (60/40 v/v, 1 mL/min flow rate). The column effluent was monitored at 295 nm (TH-EGO) and 326 nm (EDOT-EGO), referenced against a 700 nm wavelength. The data were processed using a Breeze software package (Waters). The compounds were quantified using a calibration curve obtained with standard solutions chromatographed in the same experimental conditions, with a concentration range of 1–100 μ M ($r^2 > 0.99$).

Cell lines and virus propagation. Human lung fibroblast MRC-5 (ATCC® CCL-171) and VERO E6 cells (*Cercopithecus aethiops* derived epithelial kidney, C1008; ATCC® CRL-1586) were propagated at 37°C in a humidified 5% CO₂ atmosphere in DMEM (Sigma-Aldrich) supplemented with 1% (v/v) penicillin/streptomycin solution (Sigma-Aldrich) and heat-inactivated, 10% (v/v) FBS (Sigma-Aldrich).

The human coronavirus HCoV-OC43 strain (ATCC® VR-1558) was grown as reported in Milewska *et al.*²⁶. The human β -coronavirus SARS-CoV-2, strain BetaCov/Italy/CDG1/2020|EPI

ISL 412973|2020-02-20 (GISAID accession ID: EPI_ISL_412973), was propagated on VERO E6 cells, and the infectious titer was determined by plaque assay. Virus propagation was conducted under biosafety level 3 facilities at “Istituto Superiore di Sanità” (Rome, IT).

Cytotoxicity assays. SL cytotoxicity was determined by standard 2,3-bis-(2-methoxy-4-nitro-5-sulfophenyl)-2H-tetrazolium-5-carboxanilide (XTT) for VERO E6 (Roche) or the 3-(4,5-dimethylthiazol-2-yl)-2,5-diphenyltetrazolium bromide (MTT) (Sigma-Aldrich) assay for MRC-5.

Antiviral assays against HCoV-OC43

Plaque assay. MRC-5 cells were seeded in 24-well plates and subjected to the time of addition assays with different concentrations of SL analogs or the vehicle control (DMSO), as described in the Results section. Cells were infected with HCoV-OC43 (MOI 0.1) for 2 h at 33°C, and the supernatants were then collected at 48 hpi. The extent of virus replication was subsequently assessed by titrating the infectivity of the supernatants, by standard plaque assay. Cells were fixed and stained with crystal violet solution and the absorbance readings were measured at 595 nm using a Victor X4 multilabel plate reader. Histograms were obtained by plotting the values of the 10^{-4} dilution, expressed for each compound concentration as a percentage of the mean absorbance of the uninfected control (mock) (set as 100%).

Real-Time PCR. MRC-5 cells were treated as described in the standard plaque assay section. Forty-eight hours later cells or supernatants were collected, and RNA was isolated from 200 μ l of supernatants or cell pellets, respectively, using the TRI Reagent solution (Sigma-Aldrich), according to the manufacturer’s instructions. Extracted viral RNA was retrotranscribed and amplified by the Sensi Fast Probe No Rox One step kit (Bioline). The primers and probe for N gene amplification (Eurofins Genomics) are reported in Table S1.

Western Blot analysis. Whole-cell protein extracts were prepared and subjected to Western blot analysis. The following primary antibodies were used: anti-Coronavirus mouse monoclonal antibody, HCoV-OC43 strain, clone 541-8F (MAB9012, Sigma-Aldrich), and anti-Actin (A2066, Sigma Aldrich) (both at 1:1000 dilution in 5% nonfat dry milk, TBS-Tween 0.05%).

Immunocomplexes were detected using appropriate secondary antibodies conjugated with horseradish peroxidase (HRP) (GE Healthcare Europe GmbH) and visualized by enhanced chemiluminescence (Super Signal West Pico; Thermo Fischer Scientific).

Antiviral activity against SARS-CoV-2

Plaque assay. VERO E6 cells were seeded in 24-well plates and subjected to the time of addition assays with different dilutions of SL analogs or the vehicle control (DMSO), as described in the Results sections. Cells were infected with SARS-CoV-2 (MOI 0.01) for 2 h at 37°C. After 24 h, a cytopathic effect was observed, and culture supernatants were collected for virus titration by standard TCID₅₀ assay, as previously described²⁷.

Real-Time PCR. The RNAs were tested by a TaqMan RT-PCR (Bio-Rad) to target the N genes of SARS-CoV-2, based on protocols developed by the Centers for Disease Control and Prevention (CDC; 2019-Novel Coronavirus (2019-nCoV) rRT-PCR Panel Primers and Probes. Updated: May 29, 2020). Primers and probes used (Eurofins Genomics) are reported in Table S1.

Virtual screening

EDOT-EGO and TH-EGO were evaluated by means of a structure-based virtual screening approach against all cavities of a database composed of 67 proteins and 124 corresponding pockets¹⁴. The FLAP structure-based approach²⁸ was applied to evaluate the molecular interaction fields (MIFs) complementarity between the template molecule and the cavity MIFs. The MIF superposition is reported as a complementarity score: the higher the score, the better the ligand fits into the cavity. EDOT-EGO and TH-EGO were screened against the entire database of cavities. The score values were considered for ranking the database cavities according to their complementarity with the two templates. Cavities were selected to have a Glob-prod higher than 1. Among the selected pocket we identified the orthosteric site of SARS-CoV-2 M^{pro}, which was subsequently used for docking simulations, according to the possibility of hydrolyzing SL and forming a nucleophilic adduct.

Docking simulations. Docking simulations were performed for EDOT-EGO and TH-EGO in SARS-CoV-2 M^{pro} catalytic site (PDB code: 6Y2G), using GOLD²⁹ and Glide docking from

Maestro³⁰. Static docking experiments were carried out with GOLD in both chains of the M^{pro} dimer using a spherical region of 12 Å radius and the oxygen atom of His164 as centroid, generating a maximum of 50 docking poses. According to the first catalytic step hypothesized for D14 (Figure S3), the possible covalent binding mode of the two SL in M^{pro} was further investigated through Glide CovDock procedure³¹. In this simulation, a single pose was generated for each SL, using a 22 Å cubic box region the same previously mentioned centroid.

Static docking simulations were also performed in OC43 M^{pro} catalytic site, maintaining settings similar to those previously described. Given the absence of three-dimensional information, the structure of the protein was modeled with Swiss Model, using as template 6Y2G³². Indeed, the primary sequence of the protease is quite similar, with a global identity equal to 50%, but a high similarity at the binding site level. All residues lining the pocket are conserved with the only exception of Asn142, Met165, and Pro168, respectively substituted in OC43 M^{pro} by Cys142, Leu165, and Ser168. Moreover, in SARS-CoV-2 M^{pro} (and not in OC43), Glu166 is salt-bridged to the N-terminus serine of the other monomer. Being the orientation of the mentioned amino acids biased by the conformations of 6Y2G template residues, we performed docking simulations allowing the flexibility at these residue side-chains, by means of library rotamers implemented in Gold.

SARS-CoV-2 and MERS M^{pro} purification. The SARS-CoV-2 and the Middle-East Respiratory Syndrome Coronavirus (MERS) M^{pro} proteins were expressed in *E. coli* cells BL21 (DE3) strain, the pellets were clarified by ultracentrifugation and the proteins were purified using two purification steps. Eluted fractions containing the SARS-CoV-2 M^{pro} were pooled and subjected to buffer exchange (20 mM Tris-HCl, 150 mM NaCl, 1 mM EDTA, 1 mM DTT, pH 7.8) by using Amicon Ultra 15 centrifugal filters at 4000 x g, at 4°C. The protein purity was checked by SDS-PAGE analysis.

SARS-CoV-2 and MERS M^{pro} *in-vitro* activity assays. The SARS-CoV-2 and MERS M^{pro} enzyme inhibition FRET assays^{15,33} were performed in a buffer containing 20 mM Tris (pH 7.3), 100 mM NaCl, 5 mM TCEP, 0.1% BSA, and 1 mM EDTA.

After preincubation with 15 nM of protein (a quantity below saturation for the enzymatic assay, as determined by an enzyme activity curve for M^{pro}) and different concentrations of the tested compounds for 30 minutes (or 45' and 60' in the case of longer-time experiments) at 37°C, the substrate was added (peptide DABCYL-KTSAVLQ↓SGFRKM-EDANS) and the fluorescent signal (em/ex 320/480) was monitored after 15 minutes and 30 minutes of incubation at room temperature with the substrate, for SARS-CoV-2 and MERS M^{pro}, respectively.

Statistical analysis. The statistical tests were performed using GraphPad Prism version 5.00 for Windows (GraphPad Software). The data were presented as means ± standard error of the mean (SEM). Differences were considered statistically significant for $P < 0.05$ ($P < 0.05^*$; $P < 0.01^{**}$; $P < 0.001^{***}$). CC₅₀ and IC₅₀ values were calculated by nonlinear regression (curve fitting analysis) in GraphPad Prism software.

ASSOCIATED CONTENT

Supporting Information. Supplementary Figures with additional docking analyses and the proposed mechanism of SL hydrolysis (Figures S1-S3). Supplementary Figure reporting the inhibitory effect of SL analogs on MERS-CoV M^{pro} activity (Figure S4). Tables with the extract of the virtual screening analysis (Table S1) and with the oligonucleotide sequences (Table S2).

Corresponding Author Information.

Francesca Spyrakis - Department of Drug Science and Technology, University of Turin, Via P. Giuria 9, 10125 Turin, Italy. Email: francesca.spyrakis@unito.it

Fabio Magurano - Department of Infectious Diseases, Istituto Superiore di Sanità, Viale Regina Elena 299, 00161 Rome, Italy. Email: fabio.magurano@iss.it

Valentina Dell'Oste - Department of Public Health and Pediatric Sciences, University of Turin, Via Santena 9, 10126 Turin, Italy. Email: valentina.delloste@unito.it

Acknowledgments. This research was supported by the University of Turin (PoC - TOINPROVE/2020 to VDO; by RILO2020, and RILO2021 to MDA, FG, VDO, MB (Matteo Biolatti), FS, CP, MB (Marco Blangetti), IV; by the Italian Ministry of University and Research – MUR (PRIN Project 2017ALPCM to VDO); by the “Cassa di Risparmio” of Turin Foundation [RF = 2019.2273 to VDO, RF= 2021.1745 to MB (Matteo Biolatti)]; by EU funding within the MUR PNRR Extended Partnership initiative on Emerging Infectious Diseases (Project no. PE00000007, INF-ACT to MDA and MB (Marco Blangetti); Project CH4.0 under the MUR program "Dipartimenti di Eccellenza 2023-2027" (CUP: D13C22003520001, to CP, MB (Marco Blangetti), DA, and SG).

We kindly acknowledge Molecular Discovery Ltd for providing the FLAP and BioGPS suites.

Abbreviations.

CoV: coronavirus; CC₅₀: compound concentration that produces 50% of cytotoxicity; DAD: diode-array detector; DMSO: dimethyl sulfoxide; FRET: fluorescence resonance energy transfer; HCMV: human cytomegalovirus; IC₅₀: 50% inhibitory concentration at half-maximal response; MERS: Middle-East respiratory syndrome coronavirus; MIFs: molecular interaction fields; M^{pro}: main protease; SARS-CoV-2: severe acute respiratory syndrome coronavirus-2; SLs: strigolactones.

REFERENCES

- (1) Ruiz-Aravena, M.; McKee, C.; Gamble, A.; Lunn, T.; Morris, A.; Snedden, C. E.; Yinda, C. K.; Port, J. R.; Buchholz, D. W.; Yeo, Y. Y.; Faust, C.; Jax, E.; Dee, L.; Jones, D. N.; Kessler, M. K.; Falvo, C.; Crowley, D.; Bharti, N.; Brook, C. E.; Aguilar, H. C.; Peel, A. J.; Restif, O.; Schountz, T.; Parrish, C. R.; Gurley, E. S.; Lloyd-Smith, J. O.; Hudson, P. J.; Munster, V. J.; Plowright, R. K. Ecology, Evolution and Spillover of Coronaviruses from Bats. *Nat Rev Microbiol* **2021**. <https://doi.org/10.1038/s41579-021-00652-2>.
- (2) Xiong, H.-L.; Cao, J.-L.; Shen, C.-G.; Ma, J.; Qiao, X.-Y.; Shi, T.-S.; Ge, S.-X.; Ye, H.-M.; Zhang, J.; Yuan, Q.; Zhang, T.-Y.; Xia, N.-S. Several FDA-Approved Drugs Effectively Inhibit SARS-CoV-2 Infection in Vitro. *Frontiers in Pharmacology* **2021**, *11*.
- (3) Chapman, R. L.; Andurkar, S. V. A Review of Natural Products, Their Effects on SARS-CoV-2 and Their Utility as Lead Compounds in the Discovery of Drugs for the Treatment of COVID-19. *Med Chem Res* **2022**, *31* (1), 40–51. <https://doi.org/10.1007/s00044-021-02826-2>.

- (4) Dell'Oste, V.; Spyraakis, F.; Prandi, C. Strigolactones, from Plants to Human Health: Achievements and Challenges. *Molecules* **2021**, *26* (15), 4579. <https://doi.org/10.3390/molecules26154579>.
- (5) *Strigolactones - Biology and Applications*; Koltai, H., Prandi, C., Eds.; Springer International Publishing, 2019. <https://doi.org/10.1007/978-3-030-12153-2>.
- (6) Mayzlish-Gati, E.; Laufer, D.; Grivas, C. F.; Shakhnov, J.; Sananes, A.; Bier, A.; Ben-Harosh, S.; Belausov, E.; Johnson, M. D.; Artuso, E.; Levi, O.; Genin, O.; Prandi, C.; Khalaila, I.; Pines, M.; Yarden, R. I.; Kapulnik, Y.; Koltai, H. Strigolactone Analogs Act as New Anti-Cancer Agents in Inhibition of Breast Cancer in Xenograft Model. *Cancer Biol. Ther.* **2015**, *16* (11), 1682–1688. <https://doi.org/10.1080/15384047.2015.1070982>.
- (7) Pollock, C. B.; McDonough, S.; Wang, V. S.; Lee, H.; Ringer, L.; Li, X.; Prandi, C.; Lee, R. J.; Feldman, A. S.; Koltai, H.; Kapulnik, Y.; Rodriguez, O. C.; Schlegel, R.; Albanese, C.; Yarden, R. I. Strigolactone Analogues Induce Apoptosis through Activation of P38 and the Stress Response Pathway in Cancer Cell Lines and in Conditionally Reprogrammed Primary Prostate Cancer Cells. *Oncotarget* **2014**, *5* (6), 1683–1698. <https://doi.org/10.18632/oncotarget.1849>.
- (8) Tumer, T. B.; Yilmaz, B.; Ozleyen, A.; Kurt, B.; Tok, T. T.; Taskin, K. M.; Kulabas, S. S. GR24, a Synthetic Analog of Strigolactones, Alleviates Inflammation and Promotes Nrf2 Cytoprotective Response: In Vitro and in Silico Evidences. *Comput Biol Chem* **2018**, *76*, 179–190. <https://doi.org/10.1016/j.compbiolchem.2018.07.014>.
- (9) Zheng, J.-X.; Han, Y.-S.; Wang, J.-C.; Yang, H.; Kong, H.; Liu, K.-J.; Chen, S.-Y.; Chen, Y.-R.; Chang, Y.-Q.; Chen, W.-M.; Guo, J.-L.; Sun, P.-H. Strigolactones: A Plant Phytohormone as Novel Anti-Inflammatory Agents. *Medchemcomm* **2018**, *9* (1), 181–188. <https://doi.org/10.1039/c7md00461c>.
- (10) Antika, G.; Cinar, Z. Ö.; Seçen, E.; Özbil, M.; Tokay, E.; Köçkar, F.; Prandi, C.; Tumer, T. B. Strigolactone Analogs: Two New Potential Bioactiphores for Glioblastoma. *ACS Chem Neurosci* **2022**, *13* (5), 572–580. <https://doi.org/10.1021/acscchemneuro.1c00702>.
- (11) Biolatti, M.; Blangetti, M.; D'Arrigo, G.; Spyraakis, F.; Cappello, P.; Albano, C.; Ravanini, P.; Landolfo, S.; De Andrea, M.; Prandi, C.; Dell'Oste, V. Strigolactone Analogs Are Promising Antiviral Agents for the Treatment of Human Cytomegalovirus Infection. *Microorganisms* **2020**, *8* (5), E703. <https://doi.org/10.3390/microorganisms8050703>.
- (12) Bendheim, P. E.; Poeggeler, B.; Neria, E.; Ziv, V.; Pappolla, M. A.; Chain, D. G. Development of Indole-3-Propionic Acid (OXIGON) for Alzheimer's Disease. *J Mol Neurosci* **2002**, *19* (1–2), 213–217. <https://doi.org/10.1007/s12031-002-0036-0>.
- (13) Resnick, S. J.; Iketani, S.; Hong, S. J.; Zask, A.; Liu, H.; Kim, S.; Melore, S.; Lin, F.-Y.; Nair, M. S.; Huang, Y.; Lee, S.; Tay, N. E. S.; Rovis, T.; Yang, H. W.; Xing, L.; Stockwell, B. R.; Ho, D. D.; Chavez, A. Inhibitors of Coronavirus 3CL Proteases Protect Cells from Protease-Mediated Cytotoxicity. *Journal of Virology* **2021**, *95* (14), e02374-20. <https://doi.org/10.1128/JVI.02374-20>.
- (14) Siragusa, L.; Menna, G.; Buratta, F.; Baroni, M.; Desantis, J.; Cruciani, G.; Goracci, L. CROMATIC: Cross-Relationship Map of Cavities from Coronaviruses. *J Chem Inf Model* **2022**, *62* (12), 2901–2908. <https://doi.org/10.1021/acs.jcim.2c00169>.
- (15) Owen, D. R.; Allerton, C. M. N.; Anderson, A. S.; Aschenbrenner, L.; Avery, M.; Berritt, S.; Boras, B.; Cardin, R. D.; Carlo, A.; Coffman, K. J.; Dantonio, A.; Di, L.; Eng, H.; Ferre, R.; Gajiwala, K. S.; Gibson, S. A.; Greasley, S. E.; Hurst, B. L.; Kadar, E. P.; Kalgutkar, A. S.; Lee, J. C.; Lee, J.; Liu, W.; Mason, S. W.; Noell, S.; Novak, J. J.; Obach, R. S.; Ogilvie, K.; Patel, N. C.; Pettersson, M.; Rai, D. K.; Reese, M. R.; Sammons, M. F.; Sathish, J. G.; Singh, R. S. P.; Steppan, C. M.; Stewart, A. E.; Tuttle, J. B.; Updyke, L.; Verhoest, P. R.; Wei, L.; Yang, Q.; Zhu, Y. An Oral SARS-CoV-2 Mpro Inhibitor Clinical Candidate for the Treatment of COVID-19. *Science* **2021**, *374* (6575), 1586–1593. <https://doi.org/10.1126/science.abl4784>.

- (16) Unoh, Y.; Uehara, S.; Nakahara, K.; Nobori, H.; Yamatsu, Y.; Yamamoto, S.; Maruyama, Y.; Taoda, Y.; Kasamatsu, K.; Suto, T.; Kouki, K.; Nakahashi, A.; Kawashima, S.; Sanaki, T.; Toba, S.; Uemura, K.; Mizutare, T.; Ando, S.; Sasaki, M.; Orba, Y.; Sawa, H.; Sato, A.; Sato, T.; Kato, T.; Tachibana, Y. Discovery of S-217622, a Noncovalent Oral SARS-CoV-2 3CL Protease Inhibitor Clinical Candidate for Treating COVID-19. *J Med Chem* **2022**, *65* (9), 6499–6512. <https://doi.org/10.1021/acs.jmedchem.2c00117>.
- (17) Huang, C.; Shuai, H.; Qiao, J.; Hou, Y.; Zeng, R.; Xia, A.; Xie, L.; Fang, Z.; Li, Y.; Yoon, C.; Huang, Q.; Hu, B.; You, J.; Quan, B.; Zhao, X.; Guo, N.; Zhang, S.; Ma, R.; Zhang, J.; Wang, Y.; Yang, R.; Zhang, S.; Nan, J.; Xu, H.; Wang, F.; Lei, J.; Chu, H.; Yang, S. A New Generation Mpro Inhibitor with Potent Activity against SARS-CoV-2 Omicron Variants. *Sig Transduct Target Ther* **2023**, *8* (1), 1–13. <https://doi.org/10.1038/s41392-023-01392-w>.
- (18) Yao, R.; Wang, L.; Li, Y.; Chen, L.; Li, S.; Du, X.; Wang, B.; Yan, J.; Li, J.; Xie, D. Rice DWARF14 Acts as an Unconventional Hormone Receptor for Strigolactone. *J Exp Bot* **2018**, *69* (9), 2355–2365. <https://doi.org/10.1093/jxb/ery014>.
- (19) Scaffidi, A.; Waters, M. T.; Sun, Y. K.; Skelton, B. W.; Dixon, K. W.; Ghisalberti, E. L.; Flematti, G. R.; Smith, S. M. Strigolactone Hormones and Their Stereoisomers Signal through Two Related Receptor Proteins to Induce Different Physiological Responses in Arabidopsis. *Plant Physiol* **2014**, *165* (3), 1221–1232. <https://doi.org/10.1104/pp.114.240036>.
- (20) Ramos-Guzmán, C. A.; Ruiz-Pernía, J. J.; Tuñón, I. Unraveling the SARS-CoV-2 Main Protease Mechanism Using Multiscale Methods. *ACS Catal* **2020**, *10*, 12544–12554. <https://doi.org/10.1021/acscatal.0c03420>.
- (21) Gossen, J.; Albani, S.; Hanke, A.; Joseph, B. P.; Bergh, C.; Kuzikov, M.; Costanzi, E.; Manelfi, C.; Storici, P.; Gribbon, P.; Beccari, A. R.; Talarico, C.; Spyraakis, F.; Lindahl, E.; Zaliani, A.; Carloni, P.; Wade, R. C.; Musiani, F.; Kokh, D. B.; Rossetti, G. A Blueprint for High Affinity SARS-CoV-2 Mpro Inhibitors from Activity-Based Compound Library Screening Guided by Analysis of Protein Dynamics. *ACS Pharmacol Transl Sci* **2021**, *4* (3), 1079–1095. <https://doi.org/10.1021/acspsci.0c00215>.
- (22) Spyraakis, F.; Felici, P.; Bayden, A. S.; Salsi, E.; Miggiano, R.; Kellogg, G. E.; Cozzini, P.; Cook, P. F.; Mozzarelli, A.; Campanini, B. Fine Tuning of the Active Site Modulates Specificity in the Interaction of O-Acetylserine Sulfhydrylase Isozymes with Serine Acetyltransferase. *Biochim. Biophys. Acta* **2013**, *1834* (1), 169–181. <https://doi.org/10.1016/j.bbapap.2012.09.009>.
- (23) Ma, C.; Sacco, M. D.; Hurst, B.; Townsend, J. A.; Hu, Y.; Szeto, T.; Zhang, X.; Tarbet, B.; Marty, M. T.; Chen, Y.; Wang, J. Boceprevir, GC-376, and Calpain Inhibitors II, XII Inhibit SARS-CoV-2 Viral Replication by Targeting the Viral Main Protease. *Cell Res* **2020**, *30* (8), 678–692. <https://doi.org/10.1038/s41422-020-0356-z>.
- (24) Costanzi, E.; Kuzikov, M.; Esposito, F.; Albani, S.; Demitri, N.; Giabbai, B.; Camasta, M.; Tramontano, E.; Rossetti, G.; Zaliani, A.; Storici, P. Structural and Biochemical Analysis of the Dual Inhibition of MG-132 against SARS-CoV-2 Main Protease (Mpro/3CLpro) and Human Cathepsin-L. *Int J Mol Sci* **2021**, *22* (21), 11779. <https://doi.org/10.3390/ijms222111779>.
- (25) Prandi, C.; Occhiato, E. G.; Tabasso, S.; Bonfante, P.; Novero, M.; Scarpi, D.; Bova, M. E.; Miletto, I. New Potent Fluorescent Analogues of Strigolactones: Synthesis and Biological Activity in Parasitic Weed Germination and Fungal Branching. *European Journal of Organic Chemistry* **2011**, *2011* (20–21), 3781–3793. <https://doi.org/10.1002/ejoc.201100616>.
- (26) Milewska, A.; Kaminski, K.; Ciejska, J.; Kosowicz, K.; Zeglen, S.; Wojarski, J.; Nowakowska, M.; Szczubiałka, K.; Pyrc, K. HTCC: Broad Range Inhibitor of Coronavirus Entry. *PLoS One* **2016**, *11* (6), e0156552. <https://doi.org/10.1371/journal.pone.0156552>.
- (27) Magurano, F.; Baggieri, M.; Marchi, A.; Rezza, G.; Nicoletti, L.; COVID-19 Study Group. SARS-CoV-2 Infection: The Environmental Endurance of the Virus Can Be Influenced by the

Increase of Temperature. *Clin Microbiol Infect* **2021**, 27 (2), 289.e5-289.e7.
<https://doi.org/10.1016/j.cmi.2020.10.034>.

- (28) Siragusa, L.; Luciani, R.; Borsari, C.; Ferrari, S.; Costi, M. P.; Cruciani, G.; Spyarakis, F. Comparing Drug Images and Repurposing Drugs with BioGPS and FLAPdock: The Thymidylate Synthase Case. *ChemMedChem* **2016**, 11 (15), 1653–1666.
<https://doi.org/10.1002/cmdc.201600121>.
- (29) Jones, G.; Willett, P.; Glen, R. C.; Leach, A. R.; Taylor, R. Development and Validation of a Genetic Algorithm for Flexible Docking. *J Mol Biol* **1997**, 267 (3), 727–748.
<https://doi.org/10.1006/jmbi.1996.0897>.
- (30) Friesner, R. A.; Murphy, R. B.; Repasky, M. P.; Frye, L. L.; Greenwood, J. R.; Halgren, T. A.; Sanschagrin, P. C.; Mainz, D. T. Extra Precision Glide: Docking and Scoring Incorporating a Model of Hydrophobic Enclosure for Protein-Ligand Complexes. *J Med Chem* **2006**, 49 (21), 6177–6196. <https://doi.org/10.1021/jm051256o>.
- (31) Zhu, K.; Borrelli, K. W.; Greenwood, J. R.; Day, T.; Abel, R.; Farid, R. S.; Harder, E. Docking Covalent Inhibitors: A Parameter Free Approach to Pose Prediction and Scoring. *J Chem Inf Model* **2014**, 54 (7), 1932–1940. <https://doi.org/10.1021/ci500118s>.
- (32) Waterhouse, A.; Bertoni, M.; Bienert, S.; Studer, G.; Tauriello, G.; Gumienny, R.; Heer, F. T.; de Beer, T. A. P.; Rempfer, C.; Bordoli, L.; Lepore, R.; Schwede, T. SWISS-MODEL: Homology Modelling of Protein Structures and Complexes. *Nucleic Acids Res.* **2018**, 46 (W1), W296–W303. <https://doi.org/10.1093/nar/gky427>.
- (33) Pelliccia, S.; Cerchia, C.; Esposito, F.; Cannalire, R.; Corona, A.; Costanzi, E.; Kuzikov, M.; Gribbon, P.; Zaliani, A.; Brindisi, M.; Storici, P.; Tramontano, E.; Summa, V. Easy Access to α -Ketoamides as SARS-CoV-2 and MERS Mpro Inhibitors via the PADAM Oxidation Route. *Eur J Med Chem* **2022**, 244, 114853. <https://doi.org/10.1016/j.ejmech.2022.114853>.

For Table of Contents Use Only

